RESERVOIR CHARACTERIZATION OF THE LOWER GREEN RIVER FORMATION, SOUTHWEST UINTA BASIN, UTAH

Deliverable 6.1

Generation of Geostatistical Reservoir Models

By

Milind D. Deo
University of Utah
Department of Chemical & Fuels Engineering

Contract DE-AC26-98BC15103

C. D. Morgan, Program Manager
Utah Geological Survey

Virginia Weyland, Contract Manager
U.S. Department of Energy
National Petroleum Technology Office

Submitting Organization: Utah Geological Survey
1594 West North Temple, Suite 3110
P.O. Box 146100
Salt Lake City, Utah 84114
(801) 537-3300

Disclaimer

Generation of Geostatistical Reservoir Models

Abstract

Log data (porosity and water saturation) for D and the C sandswas available at 0.5 foot intervals. The data was imported into HERESIM, a geostatistical tool. This permitted assigning constraining surfaces

Methodology

The Data

Petrophysical properties were generated in section 25 for D1-sands. Sixteen wells in the section were used. The log information included porosities and water saturations at 0.5 foot intervals. The section map with all the wells is shown in Figure 1. The map also shows the reference grid used, which was twenty blocks in the x-direction and twenty blocks in the y-direction. The block dimensions in both the x and y directions were 264 feet each.

Lithofacies Definitions and Constraining Surfaces

As a first step, lithofacies were defined based on porosities. The lithofacies definitions are provided in Table 1.

Table1-Lithofacies assignments

Porosities	Lithofacies Designation
-10-12.5	10
12.5-15	20
15-17.5	30
17.5-20 +	40

Lithofacies in four of the wells (10-25, 11-25, 12-25 and 13-25) (type logs) are shown in Figure 2. The lithofacies are bound by three surfaces. The two upper and the lower surfaces are the upper and the lower boundaries of the sand while the middle surface was chosen at the middle of each sand simply as a reference surface. A northwest-southeast crosssection through section-25 is shown in Figure 3. The surfaces for the defined cross-section are shown in Figure 4. The entire D-sand reservoir was modeled as one lithounit. A parallel grid was used in describing the stratigraphy.

Elevation of the top surface is shown in Figure 5 and the corresponding map for the bottom surface is in Figure 6. The reservoir is basically constrained between these two surfaces. The thickness distribution is shown in Figure 7. The reservoir is thickest in the central portion and tapers off at the edges.

Porosity-Permeability Relationship

Permeability was modeled using the cross-plot shown in Figure 8. A semi-logarithmic correlation between permeability and porosity was found to fit most measured porosity-permeability values across the field. The equation for the permeability-porosity cross-plot was:

$$\log(k) ? 0.218? ? 2.225$$

where, k was in millidarcies and ? was in percentage . The general statistics for the entire data set for permeability and porosity is shown in Table 2.

Table 2: General permeability and porosity statistics for the entire section.

	Lithofacies 40		Lithofacies 30		Lithofacies 20		Lithofacies 10	
Attribute	?	K(md)	?	K(md)	?	K(md)	?	K(md)
#samples	86	86	114	114	121	117	91	80
Min	15.93	17.7	15.03	11.2	12.28	2.8	10.01	0.9
Max.	20.3	158.7	17.49	38.7	16.34	21.8	12.51	3.2
Mean	18.6	74.02	16.2	21.1	13.9	6.992	11.5	2.085
Stdev	0.854	33.24	0.71	7.7	0.79	2.78	0.71	0.63

Generation of Lithotypes Fieldwide

Using the appropriate variogram parameters, lithotypes were simulated over the entire field. Lithounit distribution in the same cross-section (as in Figure 3) is shown in Figure 9. Corresponding porosities and permeabilities are shown in Figures 10 and 11.

Upscaling

At the chosen resolution, there were a total of about 250 half foot layers, which would yield a total of 100,000 grid blocks. It would be possible to build a reservoir model with these many blocks; however, the awkward aspect ratios of grid blocks is expected to cause numerical instabilities. Hence, first series of reservoir models were built by upscaling the blocks vertically. A total of 13 vertical blocks were created. The proportion of porosity as a function of elevation is shown in Figure 12. This diagram is used to select locations of upscaled layers. Upscaled layers were selected at regular intervals. The reservoir suitable for simulation was built using the upscaled information. The reservoir grid (plan view) is shown in Figure 13.

The upscaled crosssections for the section shown in Figure 3 are presented in Figures 14 (porosity), Figure 15 (permeability) and Figure 16 (water saturation). The basic quality of petrophysical property distribution is preserved in the upscaling process.

The upscaled models were later modified for the incorporation of hydraulic fractures.

The same methodology was used in generating petrophysical models for c-sands. The thicknesses, porosities, permeabilities, and water saturations are shown in Figures 17-20. The thicknesses are generally much lower than for D-sands. The porosities, permeabilities and water saturations are comparable.

The reservoir description so generated was used to simulate production in section 25 and to see if production results match the field data. Results will be provided in the reservoir simulation report.

Conclusions

The conventional log data can be used effectively to create detailed reservoir images based on geostatistics. The models need to be appropriately upscaled for use in reservoir simulation.

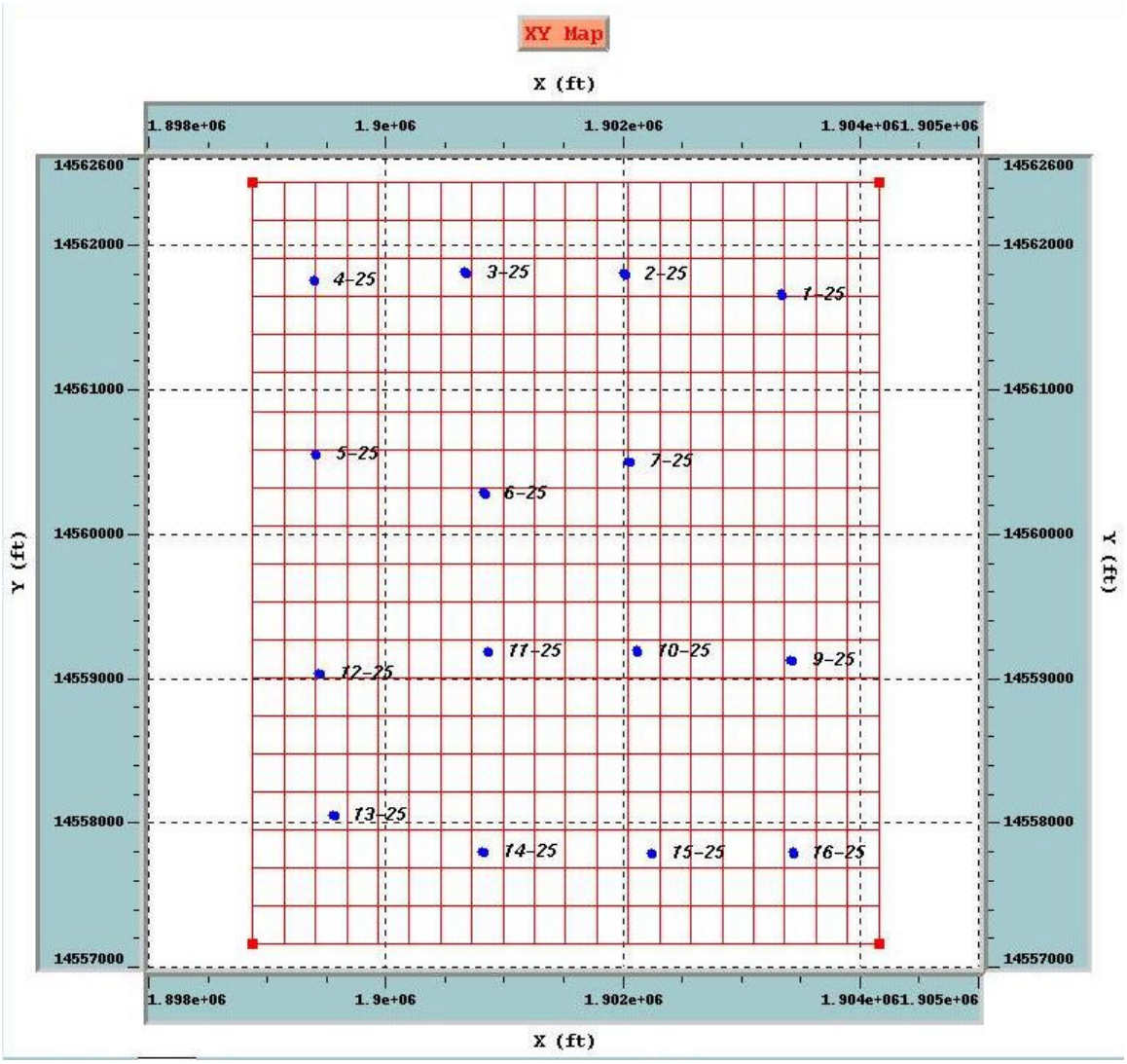

Figure 1: The map of section-25 showing the grid and all the wells

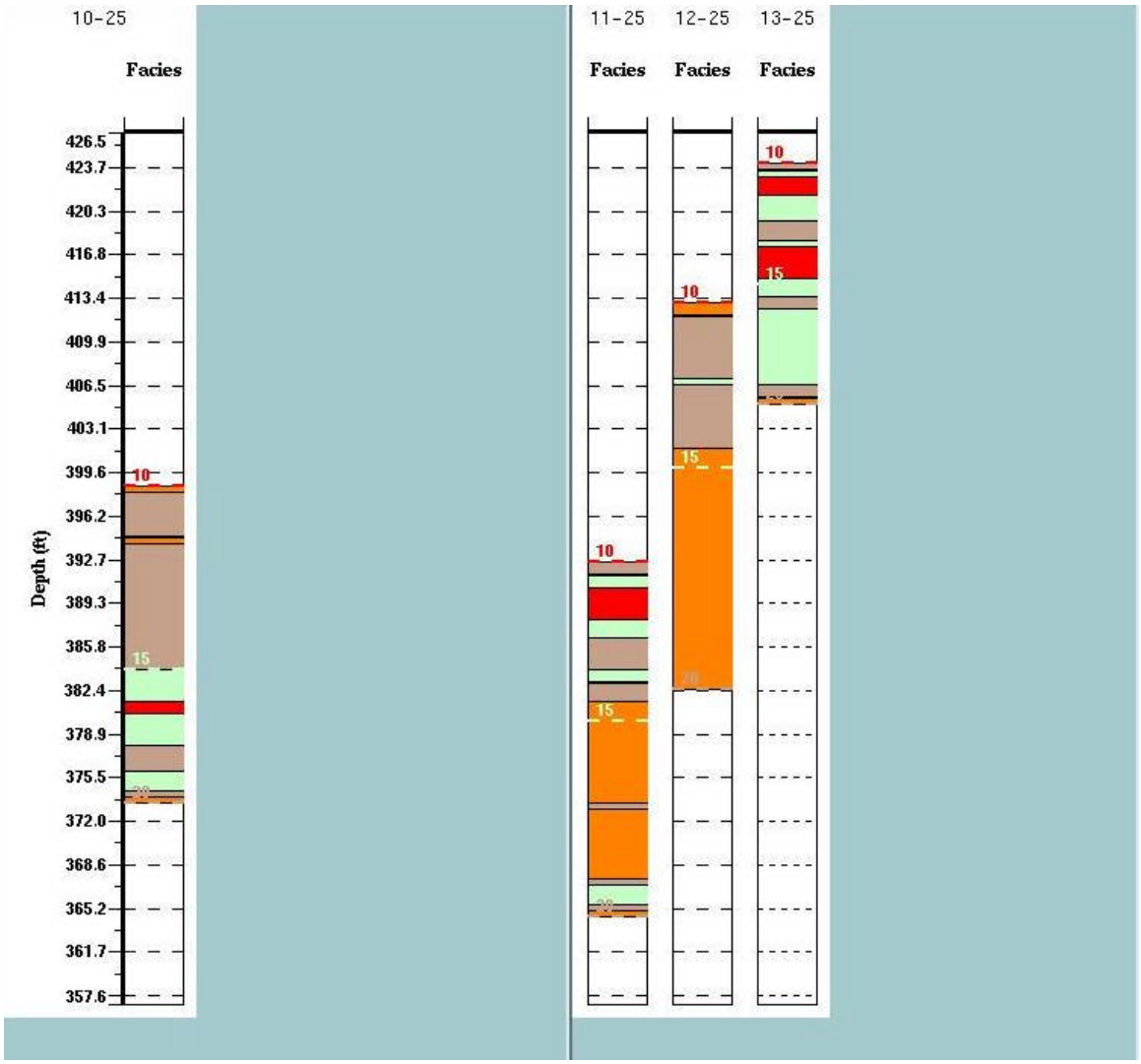

Figure 2: Lithofacies in some of the wells.

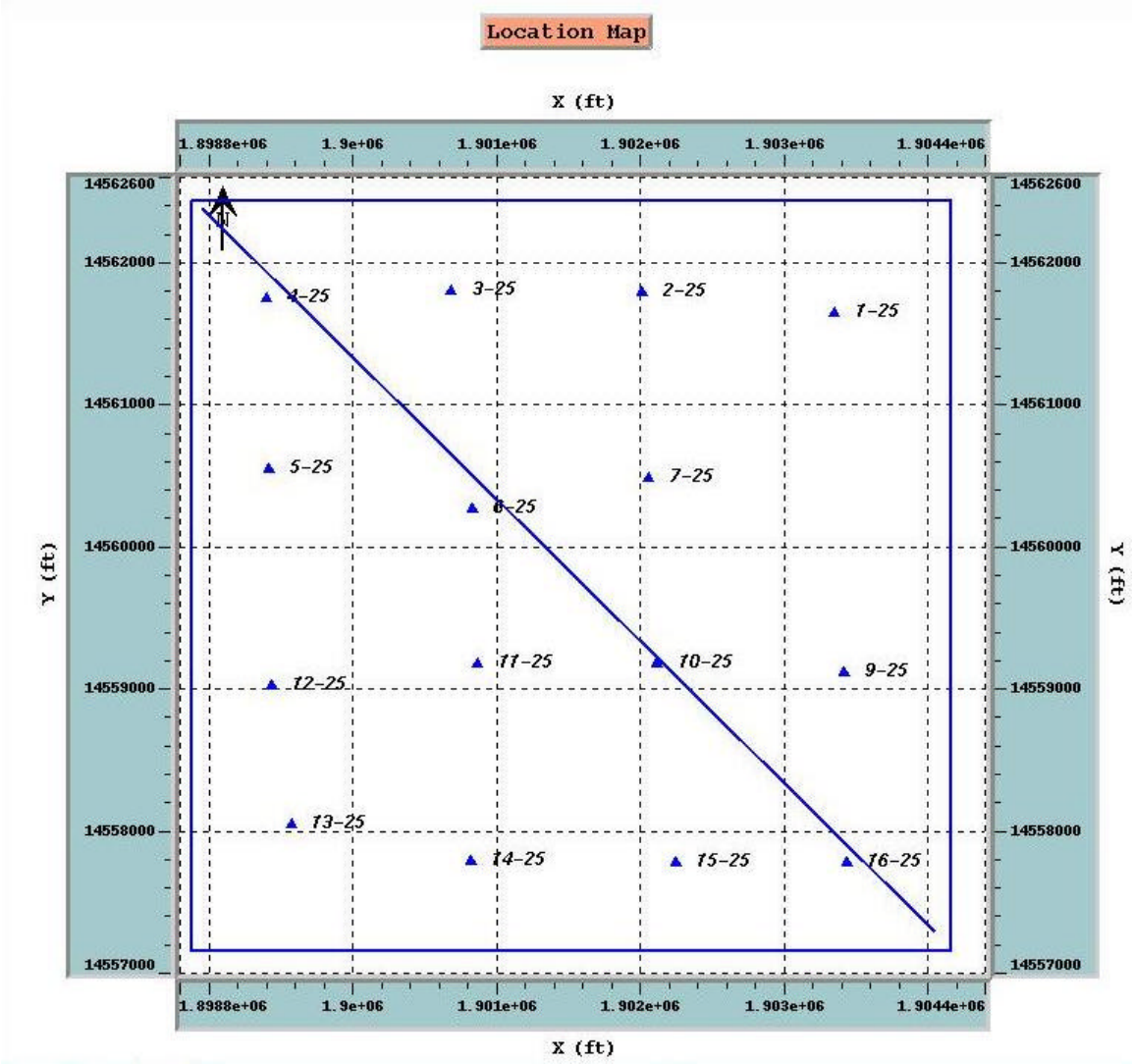

Figure 3: A northwest-southeast cross section through section 25.

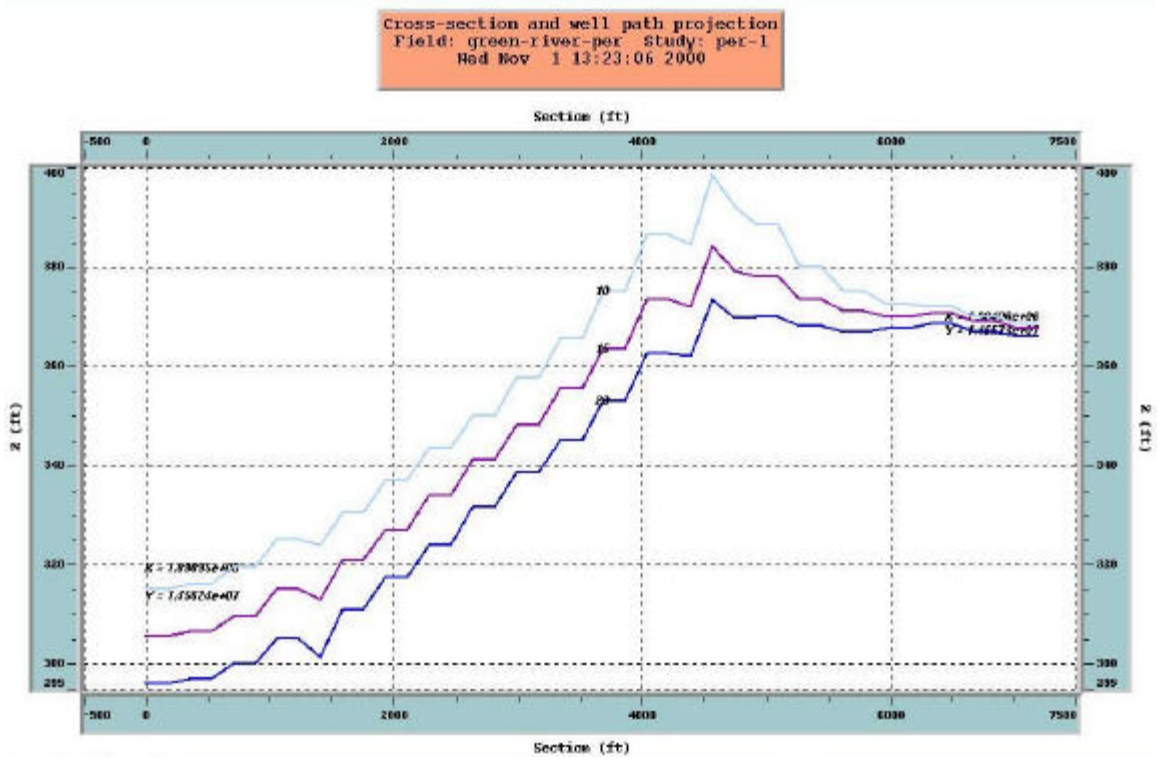

Figure 4: The three surfaces along the cross section.

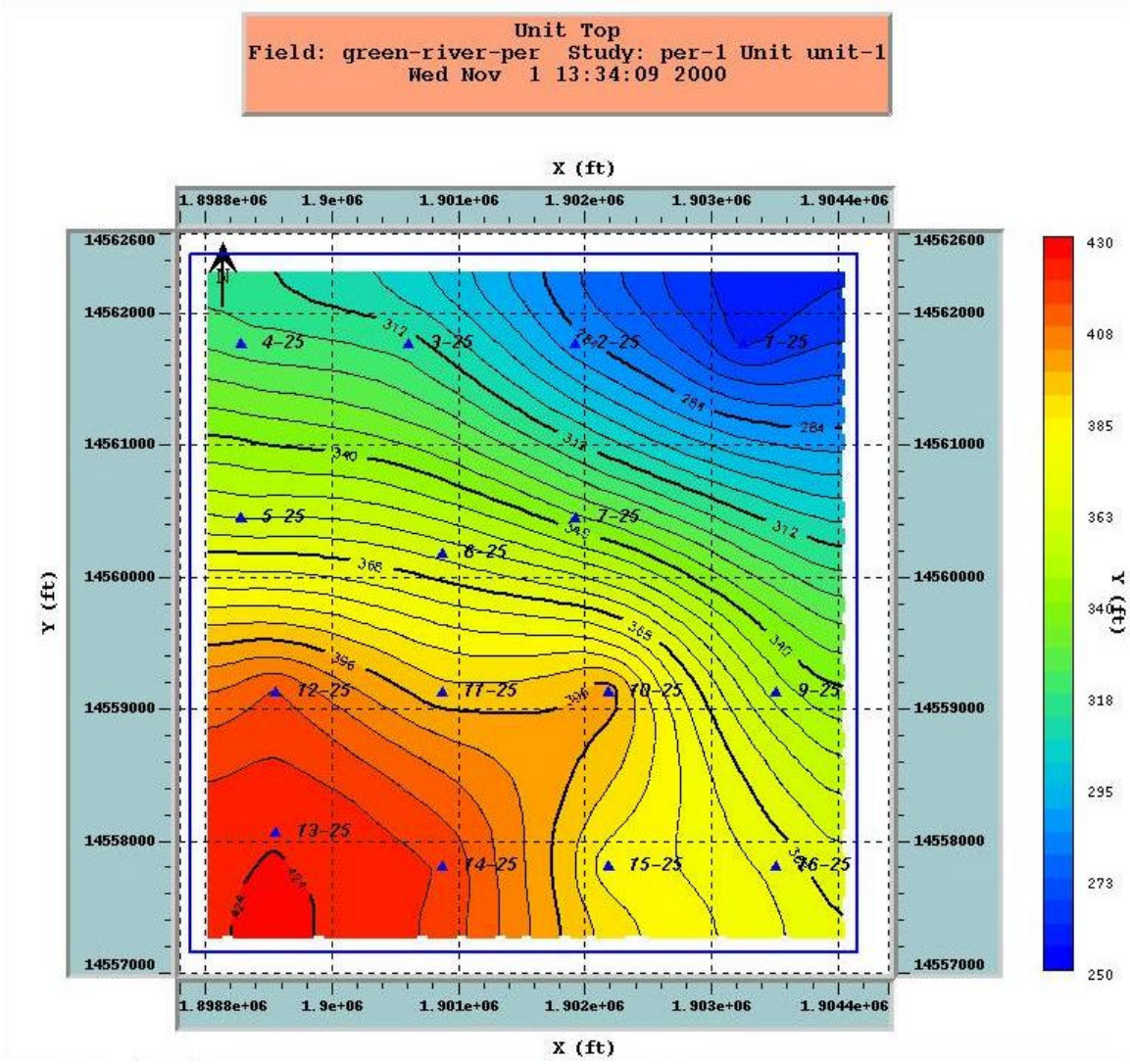

Figure 5: Contour map of the top surface. Elevations are with respect to sea level.

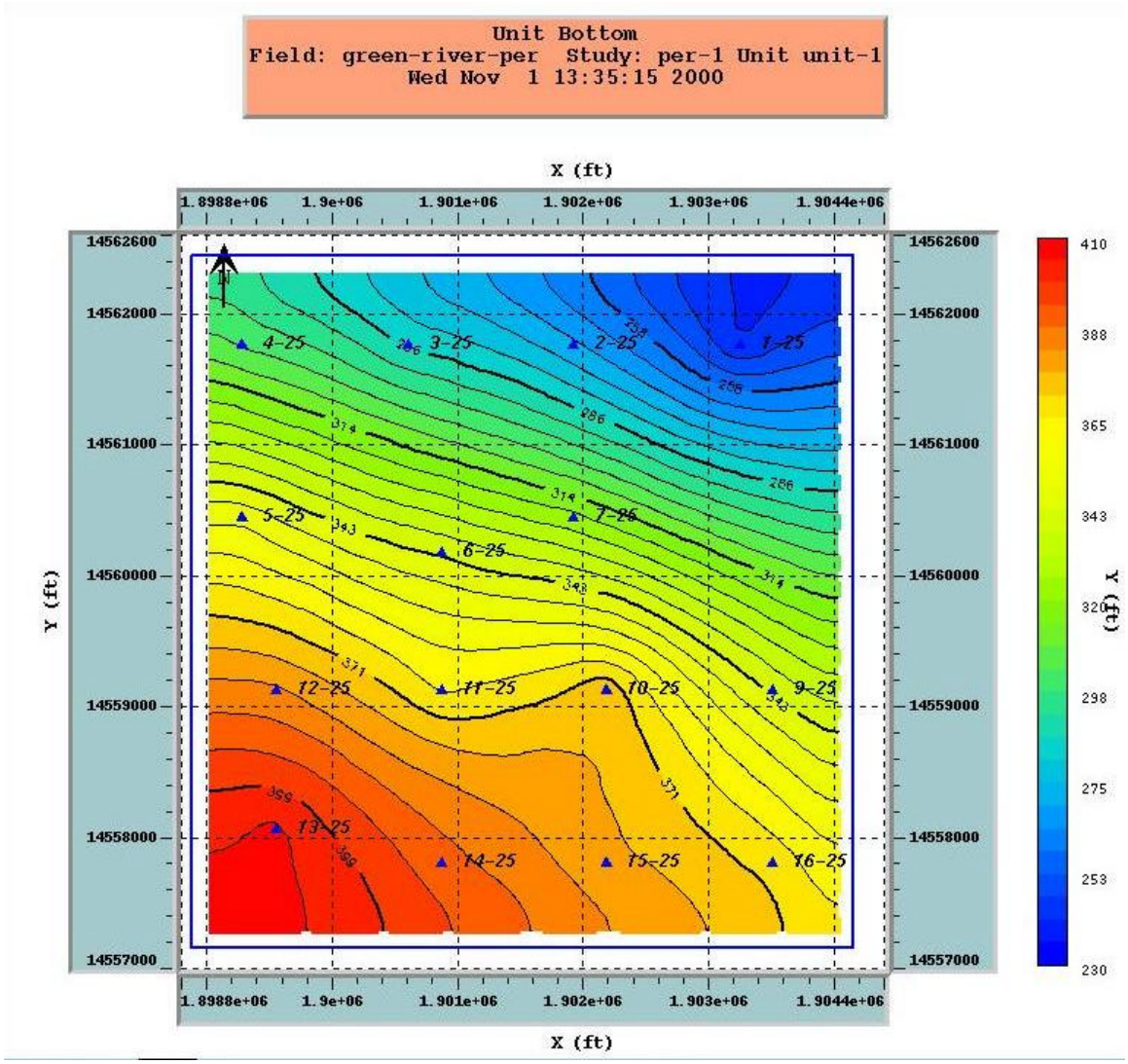

Figure 6: Contour map for the bottom of the sand. Elevations are with respect to sea level.

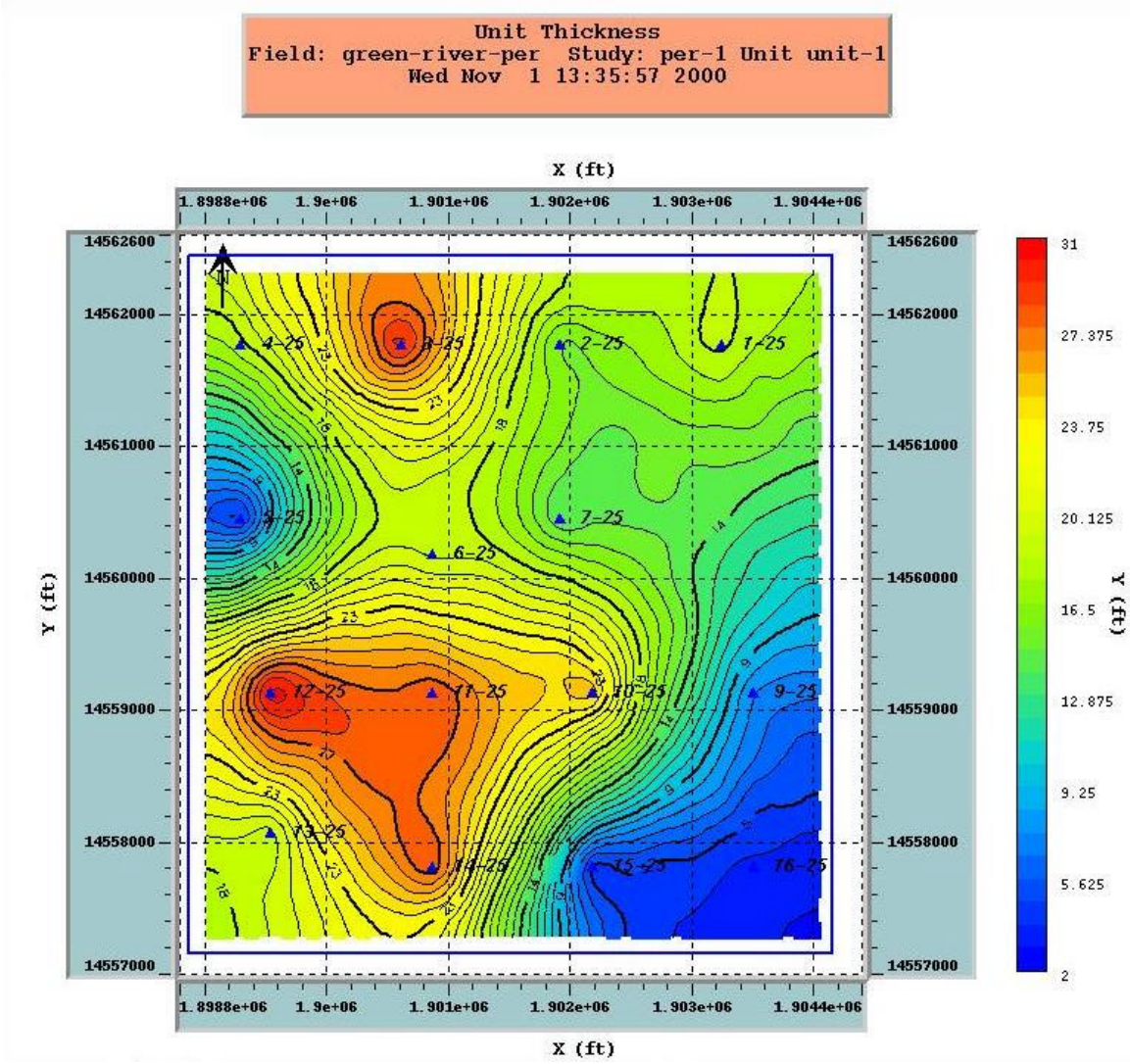

Figure 7: Sand thickness map.

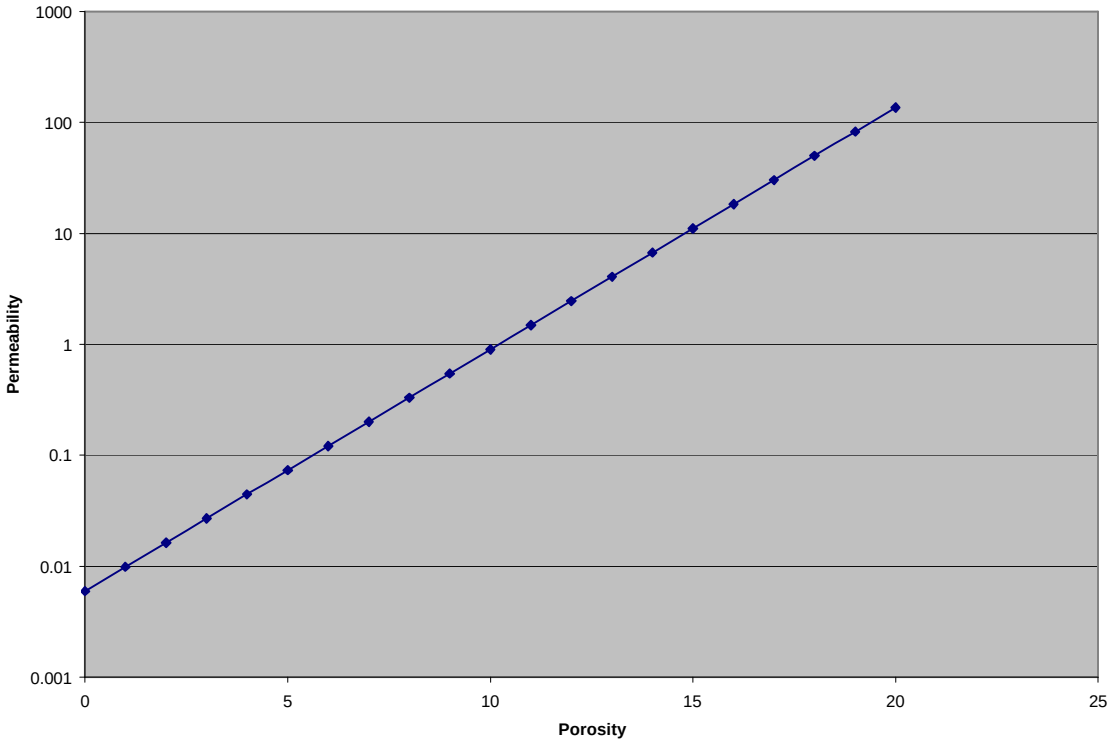

Figure 8: Porosity-permeability crossplot used in creating the petrophysical properties.

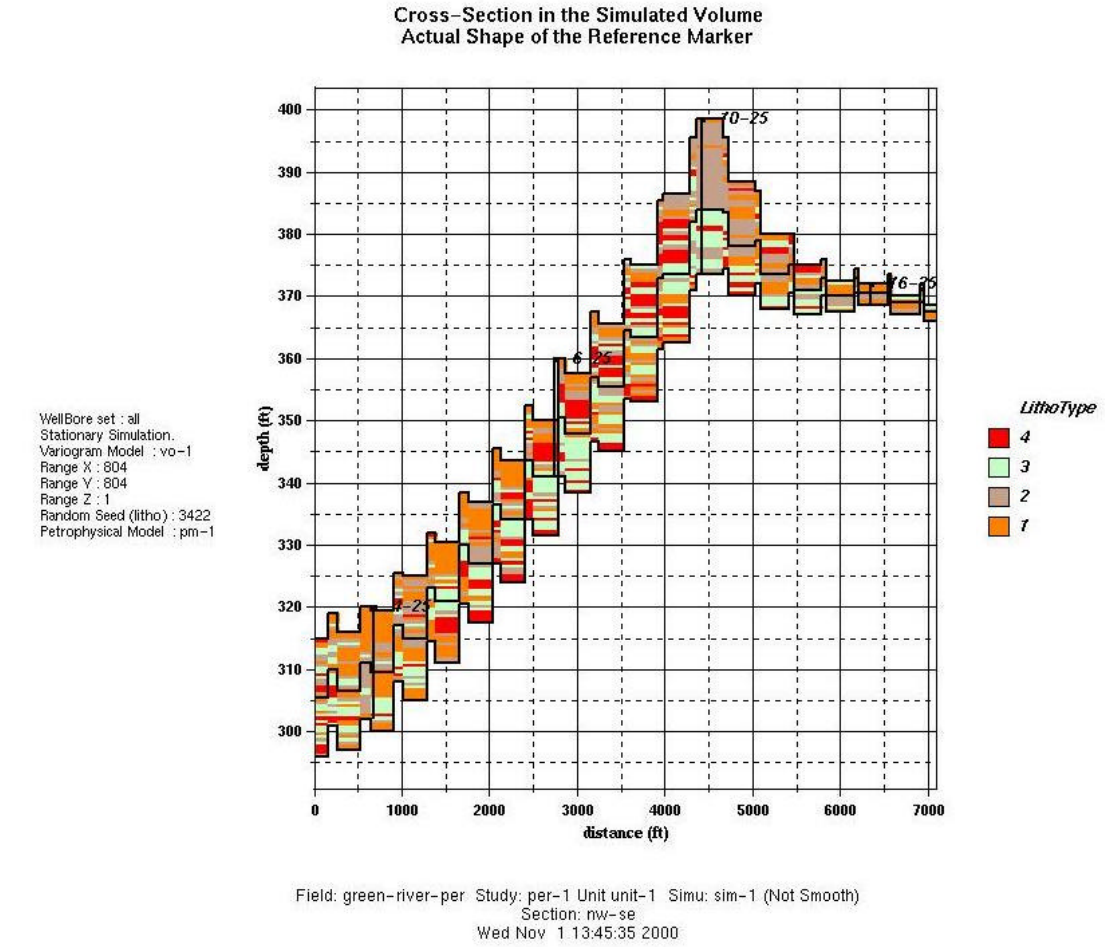

Figure 9: Lithtype distribution in the crosssection shown in Figure 3.

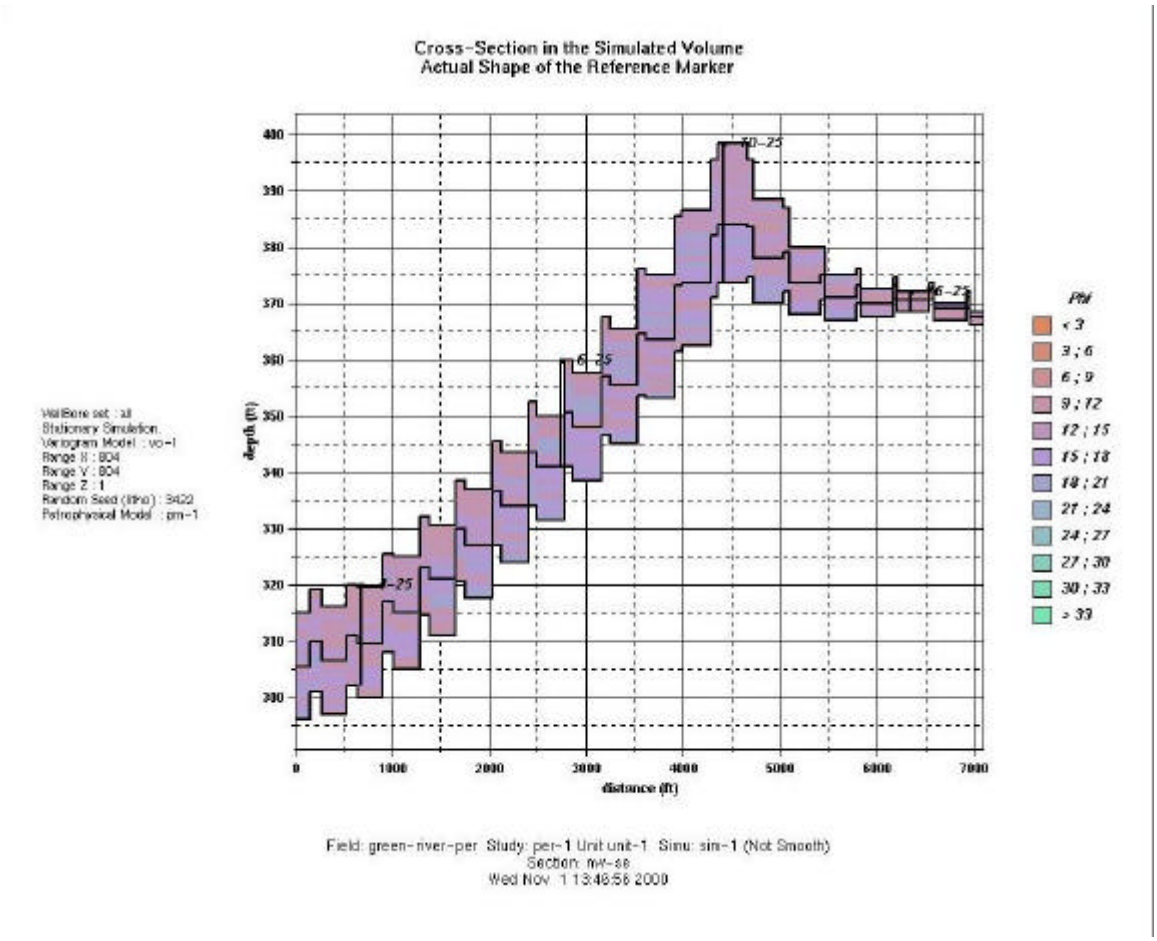

Figure 10: Porosity distribution in the croosssection shown in Figure3.

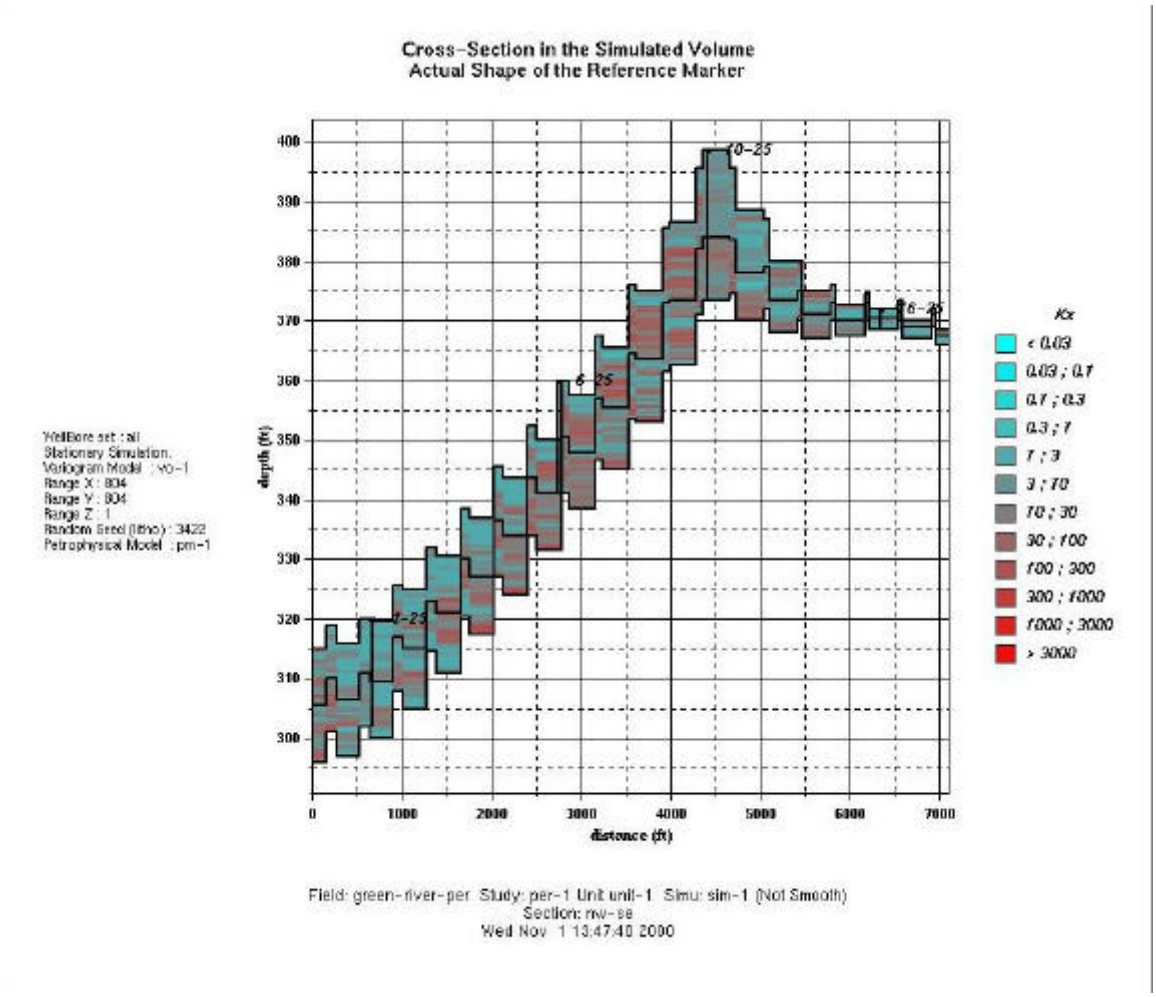

Figure 11: Permeability distribution in the crosssection shown in Figure 3.

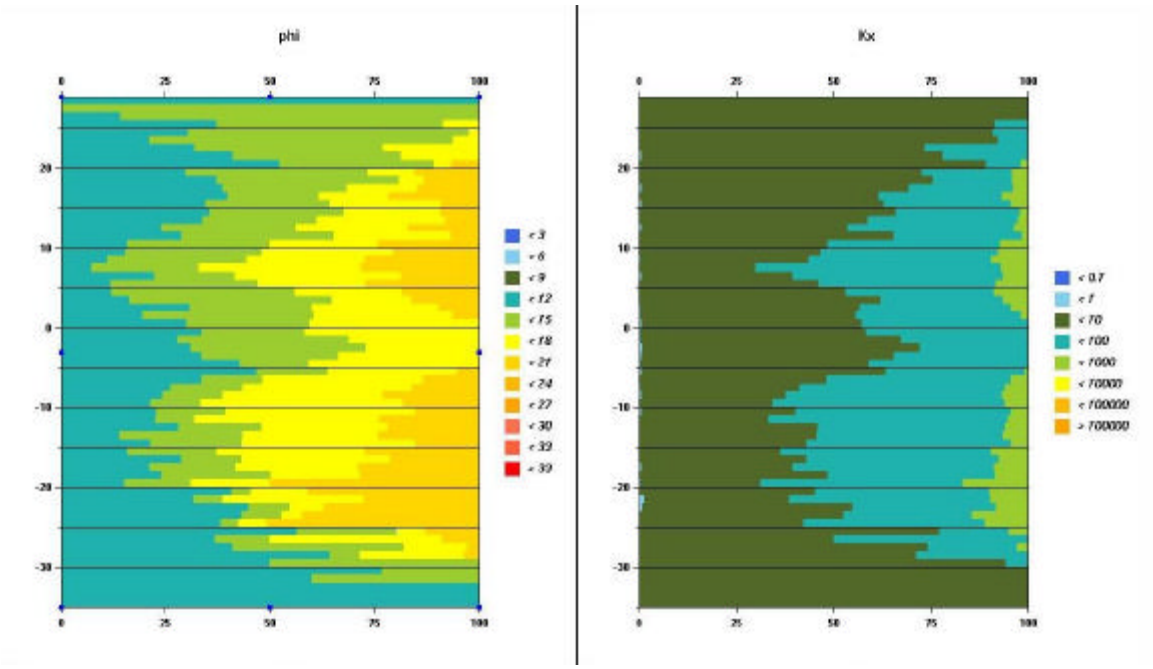

Figure 12: Porosity and permeability proportion curves and locations of upscaled layer boundaries.

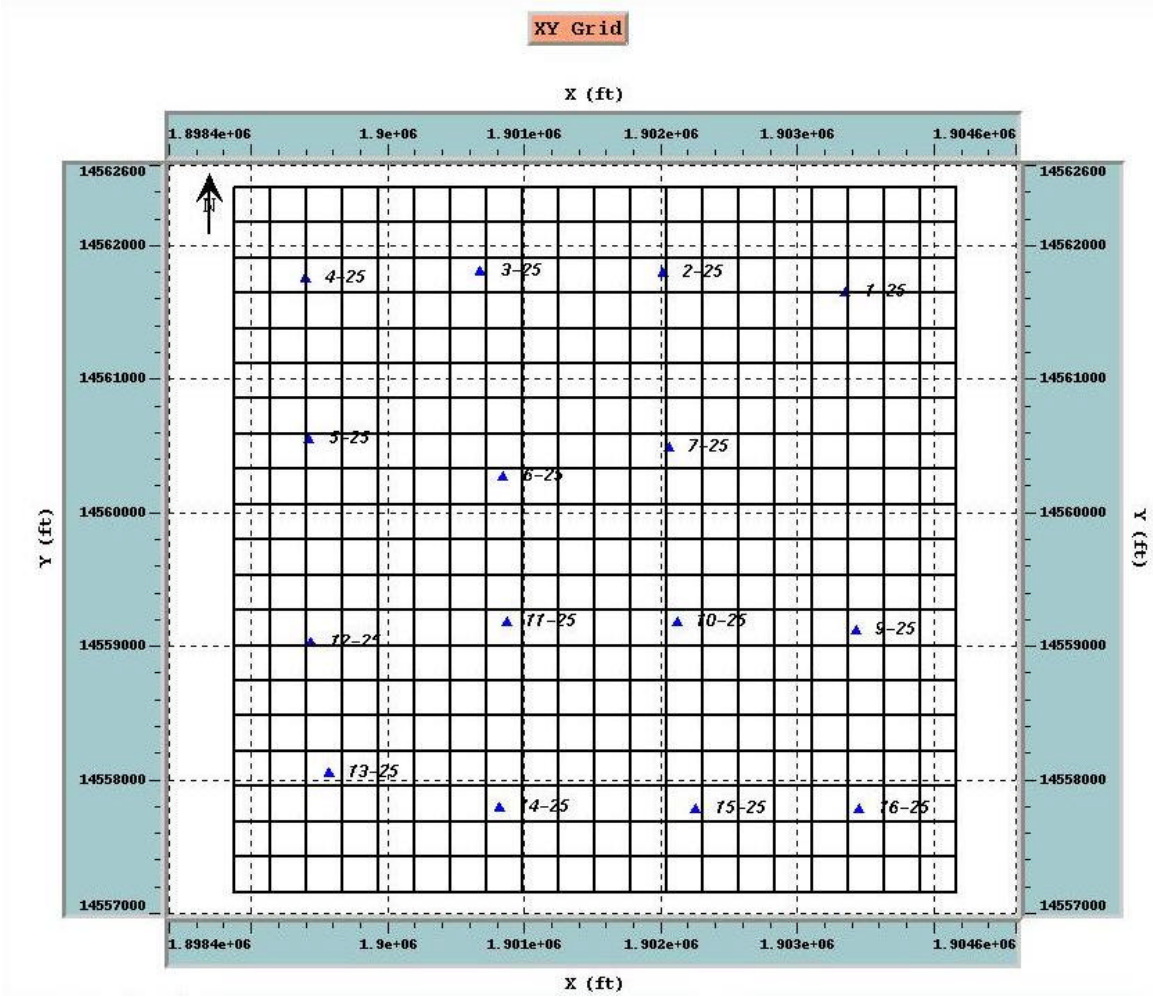

Figure 13: The plan view of the upscaled reservoir grid.

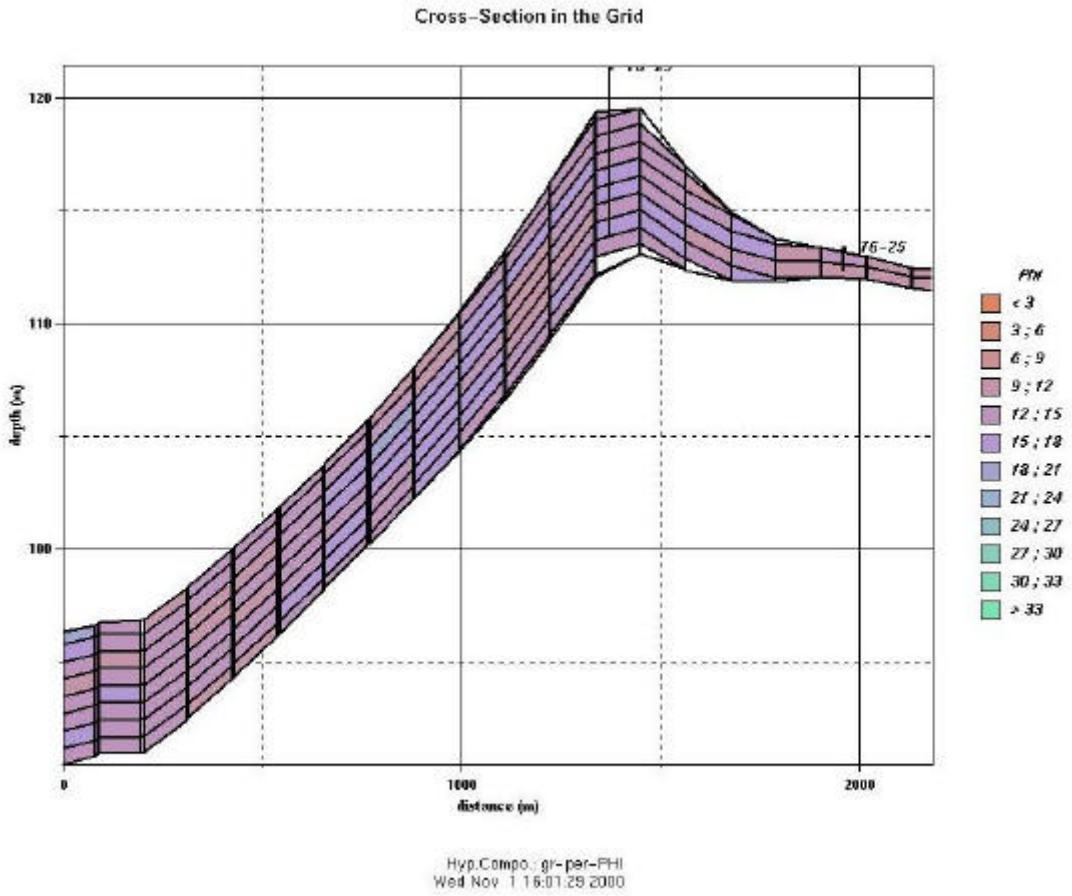

Figure 14: Porosity distribution in the crosssection shown in Figure 3 for the upscaled reservoir.

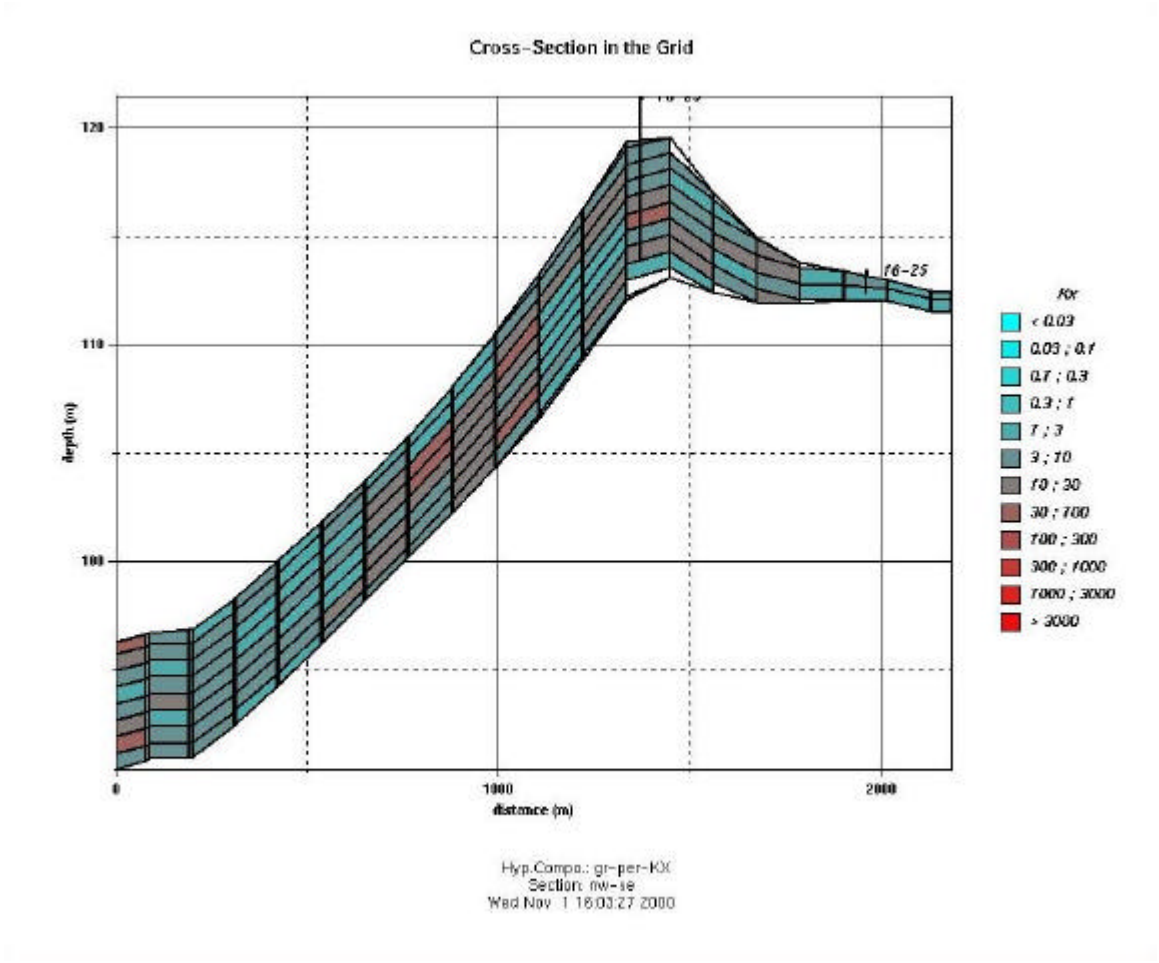

Figure 15: Permeability distribution in the upscaled reservoir for the crosssection shown in Figure 3.

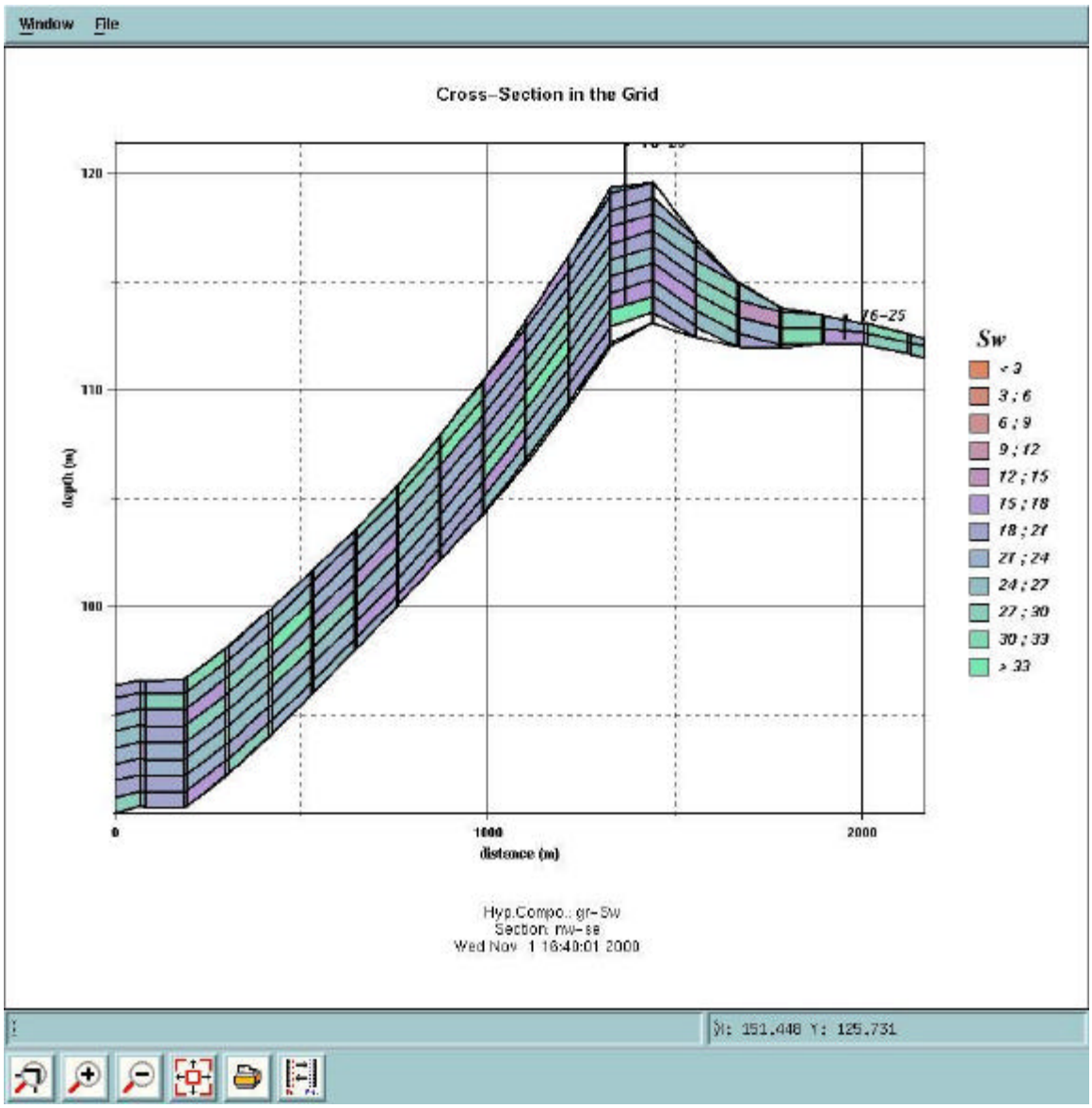

Figure 16: Water saturation distribution in the upscaled reservoir for the crosssection shown in Figure 3.

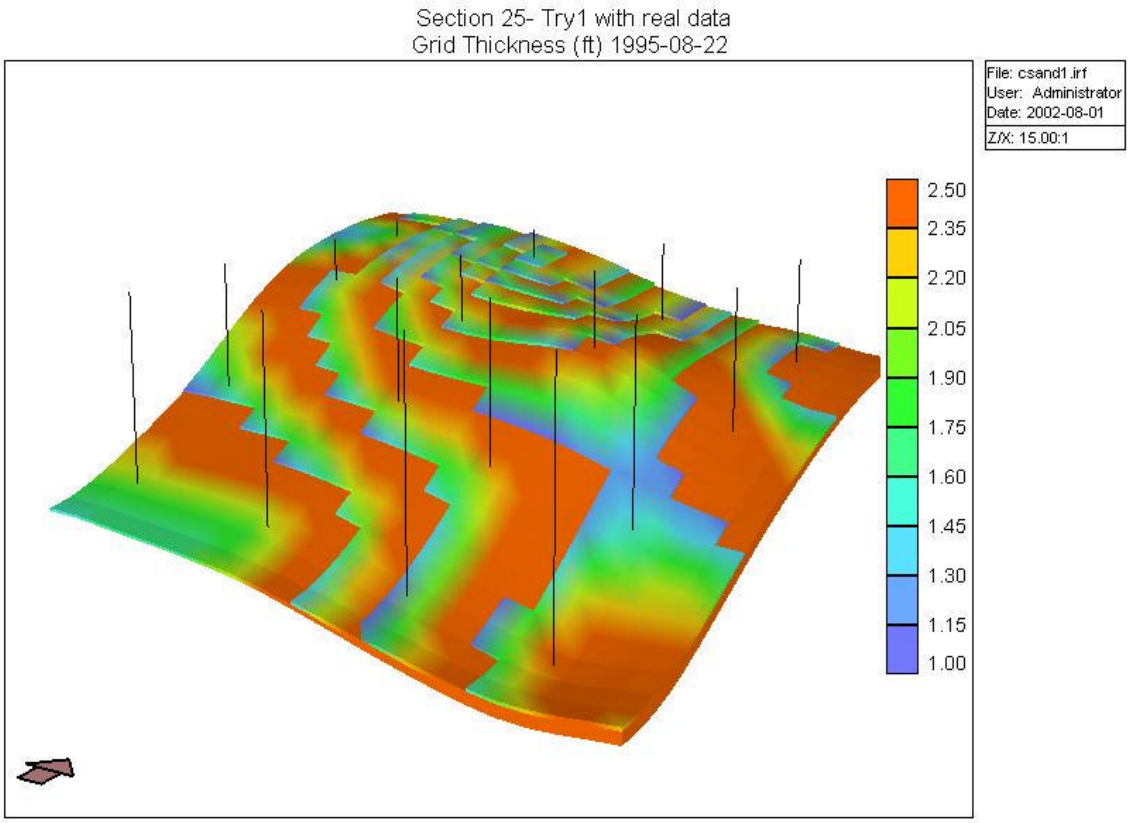

Figure 17: The C-sand thickness map.

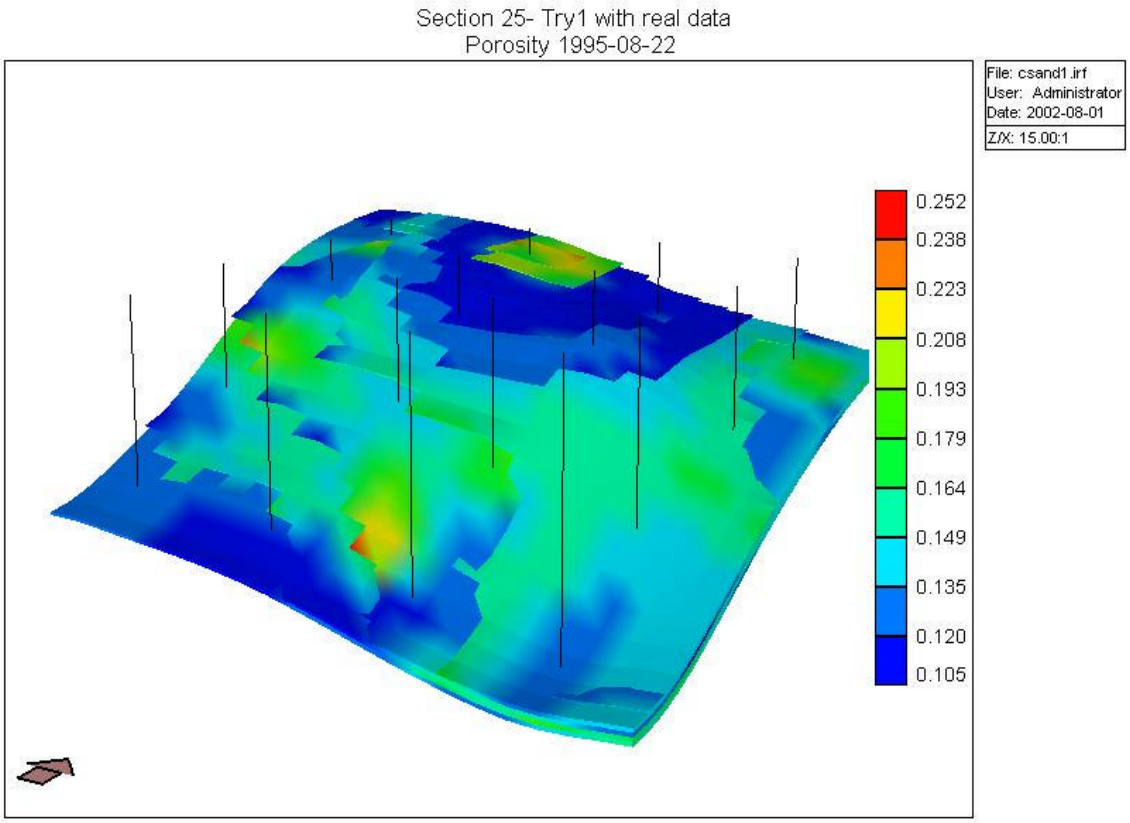

Figure 18: The C-sand porosity map.

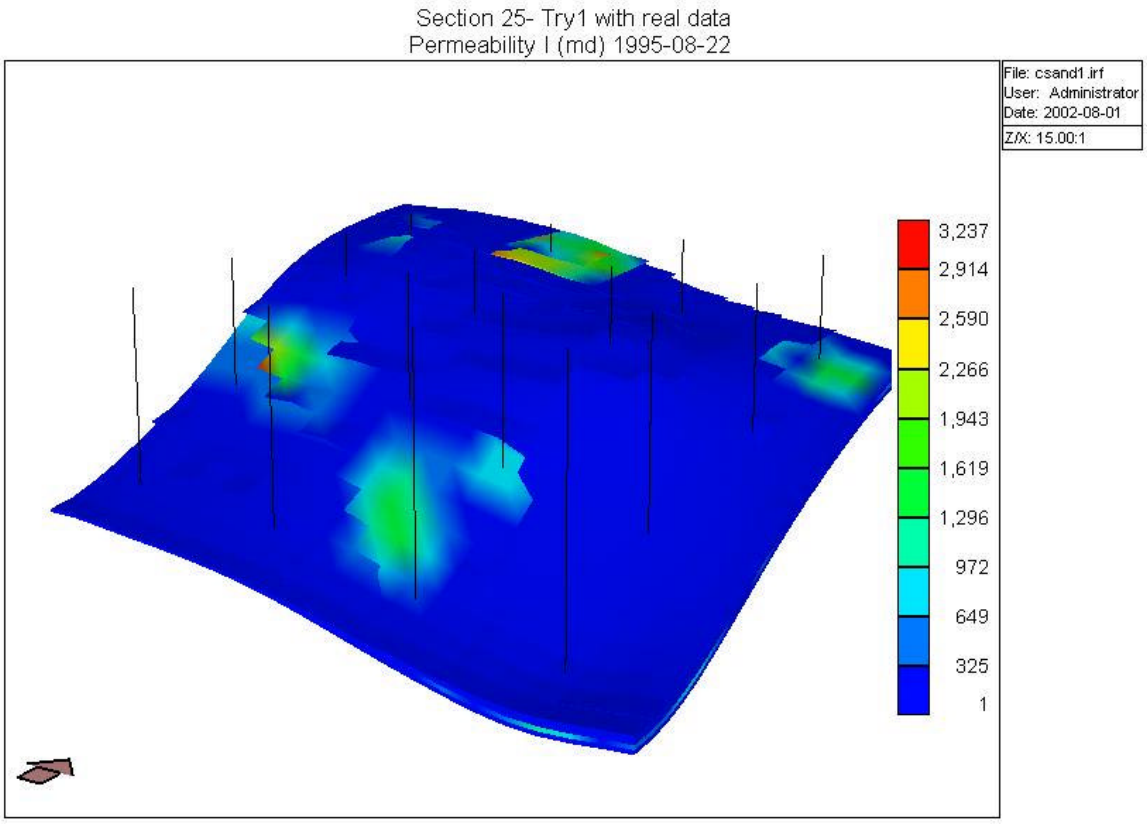

Figure 19: The C-sand permeability values.

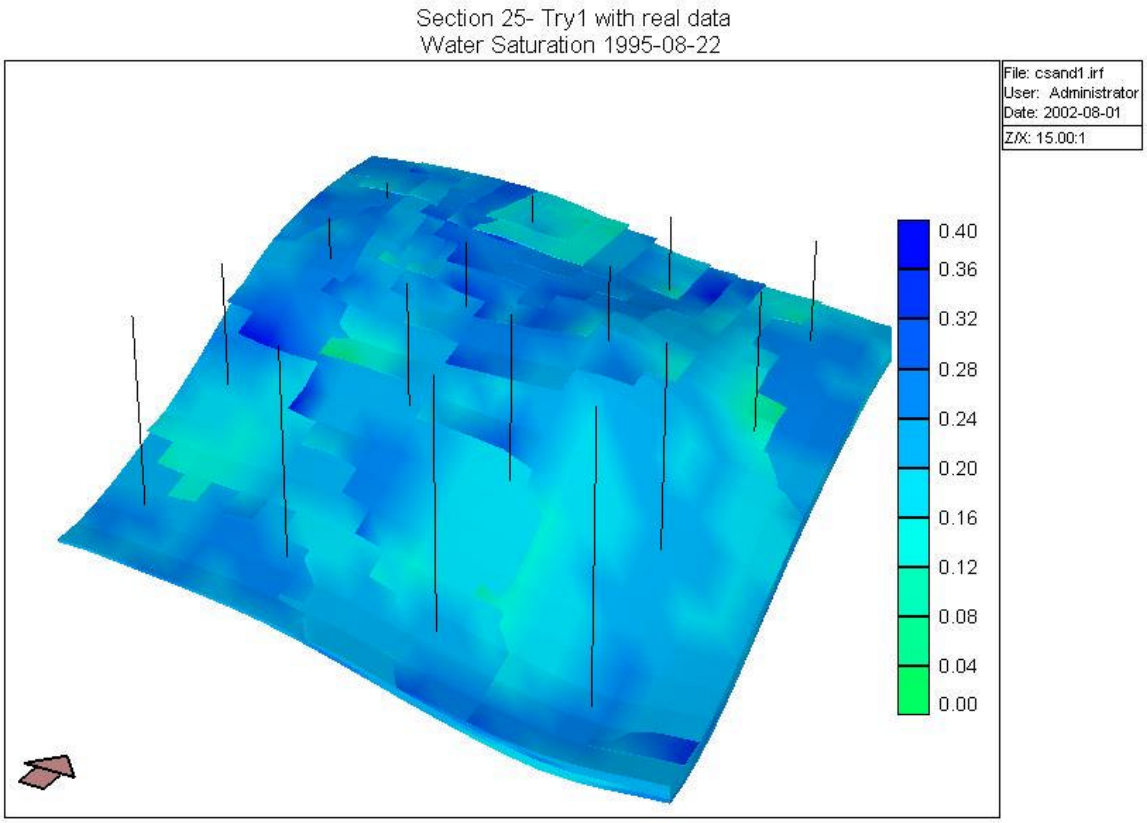

Figure 20: C-sand water saturations.